

Inclusive η' Production From The $\Upsilon(1S)$

Abstract

The large rate for $B \rightarrow X_s \eta'$ could be explained by an exotic QCD process that would also be present in $\Upsilon(1S)$ decays, especially at large η' energies. To test this hypothesis, we present the measurement of the η' energy spectrum dN/dZ ($Z = E_{\eta'}/E_{beam}$). The shape of the η' spectrum is not purely exponential and may indicate the presence of more than one production process. We set an upper limit for the $\Upsilon(1S) \rightarrow \eta' X$ branching fraction in the higher Z range ($Z > 0.7$).

1 Introduction

One of the processes that might explain the large $B \rightarrow \eta' X_s$ rate measured by CLEO [1], is $b \rightarrow s(g^* \rightarrow g\eta')[2, 3, 4]$, where the coupling is large. The effective $\eta' g^* g$ coupling can be written as [5]

$$H(q^2) \varepsilon_{\alpha\beta\mu\nu} q^\alpha k^\beta \varepsilon_1^\mu \varepsilon_2^\nu, \quad (1)$$

where $q = p_b - p_s$ is the (g^*) virtual gluon's four-momentum, k is the (g) "on-shell" gluon's momentum, and $H(q^2)$ is the $g^* g \eta'$ transition form factor. Several authors have [5, 6] suggested that the region of the q^2 relevant in the process $b \rightarrow s g \eta'$, can also be accessed in fast η' production in $\Upsilon(1S)$. Thus constraints can be put on the $H(q^2)$ from the η' spectrum in $\Upsilon(1S)$ decays. These suggestions motivated our analysis. Three possible models for the q^2 dependence of this form factor are illustrated in Figure 1.

The theoretical predictions referred to in this paper are made assuming that all $\Upsilon(1S)$ decays are into three gluons (ggg). In order to compare our measurement to them we have to correct for the $q\bar{q}$ contribution in $\Upsilon(1S)$ decays. We estimate

$$\mathcal{B}(\Upsilon(1S) \rightarrow \gamma \rightarrow q\bar{q}) = R \cdot \mathcal{B}(\Upsilon(1S) \rightarrow \mu\mu) = (8.8 \pm 0.3)\%, \quad (2)$$

where $R_{\sqrt{s} \approx 9.5} = 3.56 \pm 0.07$ [7] and the $\mathcal{B}(\Upsilon(1S) \rightarrow \mu\mu)$ is taken as $(2.48 \pm 0.06)\%$.

Although several processes can contribute to inclusive η' production in $\Upsilon(1S)$ decays, it is believed that the soft processes including fragmentation populate only the low q^2 or equivalently the low Z region, where

$$Z \equiv E_{\eta'}/E_{beam} = 2E_{\eta'}/M(\Upsilon(1S)). \quad (3)$$

Thus in the large Z region significant η' production would indicate a large $\eta' g^* g$ coupling. The ARGUS collaboration had an integrated luminosity of 32 pb^{-1} on the $\Upsilon(1S)$ resonance. In a recent talk A. Kagan [5] cites the upper limit in the higher Z region $\mathcal{B}_{Z>0.7}(\Upsilon(1S) \rightarrow \eta' X) < (6.5 \pm 1.3) \times 10^{-4}$, where he extracted the number from an unpublished thesis [8]), where no continuum subtraction was attempted. While the theoretical predictions are calculated for

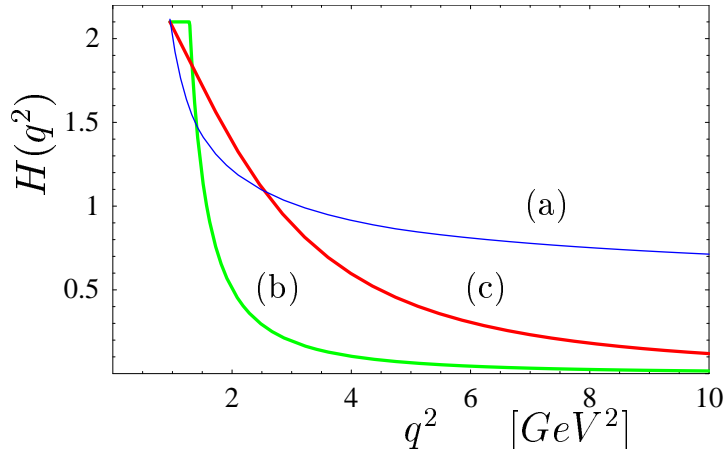


Figure 1: There are three choices for the form factor $H(q^2)$: (a) the slowly falling form factor, (b) a rapidly falling form factor representative of perturbative QCD calculations, (c) an intermediate example (adopted from [5]).

“direct” $\Upsilon(1S)$ hadronic decays, i.e. excluding $\Upsilon(1S) \rightarrow q\bar{q}$ events, and essentially leaving only ggg events, the ARGUS data includes all $\Upsilon(1S)$ decay channels as well as contribution from continuum events are not subtracted. Also, in order to see the η' signal they had to make a very hard cut on the η' momentum ($P_{\eta'} > 1$ GeV) and thus had to model the η' momentum spectrum. CLEO data is of a much better quality, so that such hard cuts are not necessary, and there is enough statistics available in order to subtract the continuum.

2 Data Sets and Selection Criteria

In this study we use CLEO II data recorded at the $\Upsilon(1S)$ resonance (9.46 GeV), a total of 80 pb^{-1} from 1S1, 1S2, and 1S3 dataset hadronic skims. The number of $\Upsilon(1S)$ events is estimated to be 1.862×10^6 (We count the total number of hadronic events and use the efficiencies in CBX 98-16 to derive the number of $\Upsilon(1S)$ [9]). We use off-resonance continuum data collected below $\Upsilon(4S)$ resonance (10.52 GeV) to estimate the contribution of continuum events. Since we need to subtract continuum and estimate the $\Upsilon(1S) \rightarrow q\bar{q}$ contribution, we use 4S2-4S7, 4SE-4SG continuum data, with a total integrated luminosity about 1200 pb^{-1} .

In reconstructing η' we use only one decay channel: $\eta' \rightarrow \eta\pi^+\pi^-$ with a branching fraction of 44%, and $\eta \rightarrow \gamma\gamma$ with a branching fraction of 39%. For η reconstruction, we use the XBAL package and constrain the two photons to have the invariant mass of the η . The photons are required to be from the good barrel region only. For η 's coming from low energy η' candidates ($Z < 0.5$) the photons are required not to be from a possible π^0 . Here Z is defined as $E_{\eta'}/E_{beam}$ for $\Upsilon(1S)$ data; We use a slightly modified definition for off-resonance data which will be explained in next section. The detailed selection criteria are shown in Table 1.

The $\eta\pi^+\pi^-$ invariant mass spectra are shown in Figure 2 for $\Upsilon(1S)$ data and Figure 3 for off-resonance continuum data. The spectra are fit with a Gaussian function for signal and second order polynomial function for background. The numbers of reconstructed η' are extracted from

Photon	Minimum energy:	EBUMP > 30 MeV
	From good barrel:	$ \cos \theta < 0.707$
	EM-like shower shape:	E925U > C92501
	Not from a shower fragment:	IBSTOP = 0
	Not from charged track:	ANGCRT > 20°
η	Invariant mass cut:	$ M_{\gamma\gamma} - M_{\eta} < 3\sigma$
	If both photon are from connected regions, they are from same region	
	Invariant mass constraint kinematic fit	
	π^0 veto on photon for low energy η' ($Z < 0.5$)	
π^{\pm}	TNG approval	TRACKMAN ≥ 0
	Good primary track	KINCD = 0
	Impact point cut ($p \leq 0.25$ GeV):	$ DBCD < 1.0$ cm, $ Z0CD - ZVPTX < 5$ cm
	Impact point cut ($p > 0.25$ GeV):	$ DBCD < 0.5$ cm, $ Z0CD - ZVPTX < 3$ cm
	dE/dX consistence with π	$ SGPIDI < 3$

Table 1: Selection criteria for η' reconstruction

the fit. We find 1486 ± 137 η' from the $\Upsilon(1S)$ data, and 4062 ± 174 η' from the off-resonance data.

In order to measure the Z spectrum we also reconstruct η' in Z intervals as shown in Figure 4 and Figure 5 for $\Upsilon(1S)$ and off-resonance data, respectively. We choose the Z interval as 0.1. The invariant mass spectrum are fit with the same function as for overall Figures 2 and 3. To reduce uncertainty due to the fit especially for high energy η' , we fix the mass of the η' to our average value over all Z; the Monte Carlo shows that the mass measurement is independent of η' energy. We extract the width of the Gaussian distribution from MC and perform a smooth fit as a function of Z. The smoothed values are used in the fit as a fixed parameter.

3 MC Simulation

The hadronic events at $\Upsilon(1S)$ energy arise from different categories: about 4 nb comes from $q\bar{q}$ decayed from continuum e^+e^- collisions, about 2 nb from $\Upsilon(1S) \rightarrow \gamma \rightarrow q\bar{q}$, 18 nb from ggg , and 0.5 nb from γgg from the $\Upsilon(1S)$. The first two have same event topology and reconstruction efficiency. We use the $q\bar{q}$ generator (model 11) to simulate these events. The γgg events are similar to that of ggg and have a relatively small cross-section; thus we treat them the same way as ggg events. We use the ggg generator (model 12) to simulate this part.

We rely on off-resonance continuum data to estimate the $q\bar{q}$ contribution in $\Upsilon(1S)$ data. However, the continuum data were taken for continuum subtraction in $\Upsilon(4S)$ studies. The center of mass (CM) energy ($E_{\text{CM}} = 10.52$ GeV) is close to $\Upsilon(4S)$ mass (10.58 GeV), but more than 1 GeV higher than $\Upsilon(1S)$ mass (9.46 GeV). The difference of reconstruction efficiency due to this energy difference is not negligible. We thus use different $q\bar{q}$ simulations for continuum data and $\Upsilon(1S)$ data.

The energy difference also affects the Z spectrum of η' from continuum MC as shown in Figure 6-(a). The solid line is the $E_{\eta'}/E_{\text{beam}}$ distribution for the $\Upsilon(1S)$ data ($E_{\text{CM}} = 9.46$

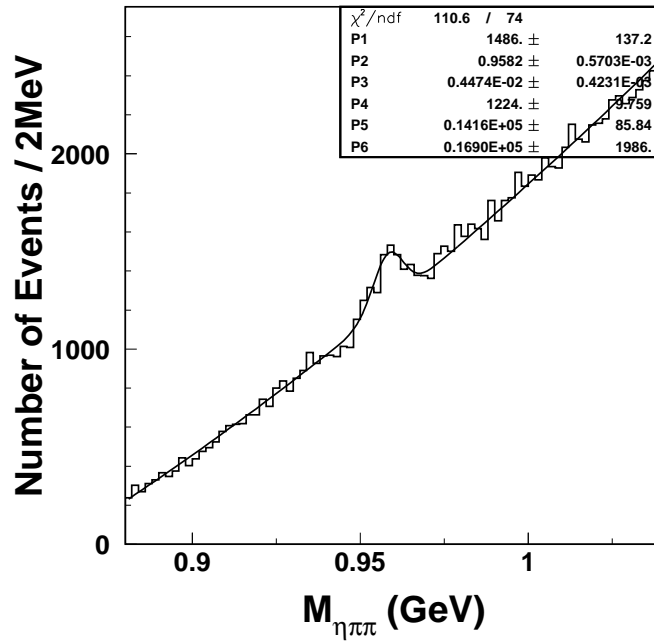


Figure 2: The $\eta\pi^+\pi^-$ invariant mass spectrum reconstructed from $\Upsilon(1S)$ data, fit with Gaussian function for signal and second order polynomial for background.

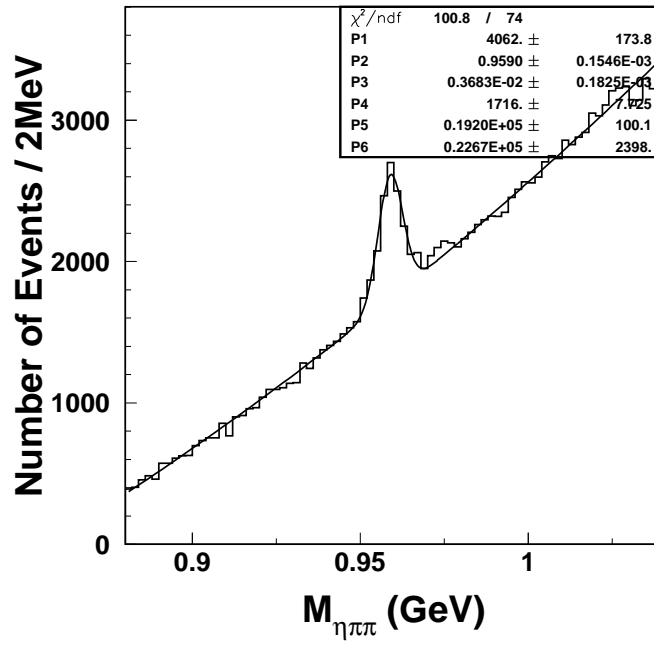


Figure 3: The $\eta\pi^+\pi^-$ invariant mass spectrum reconstructed from off-resonance data, fit with Gaussian function for signal and second order polynomial for background.

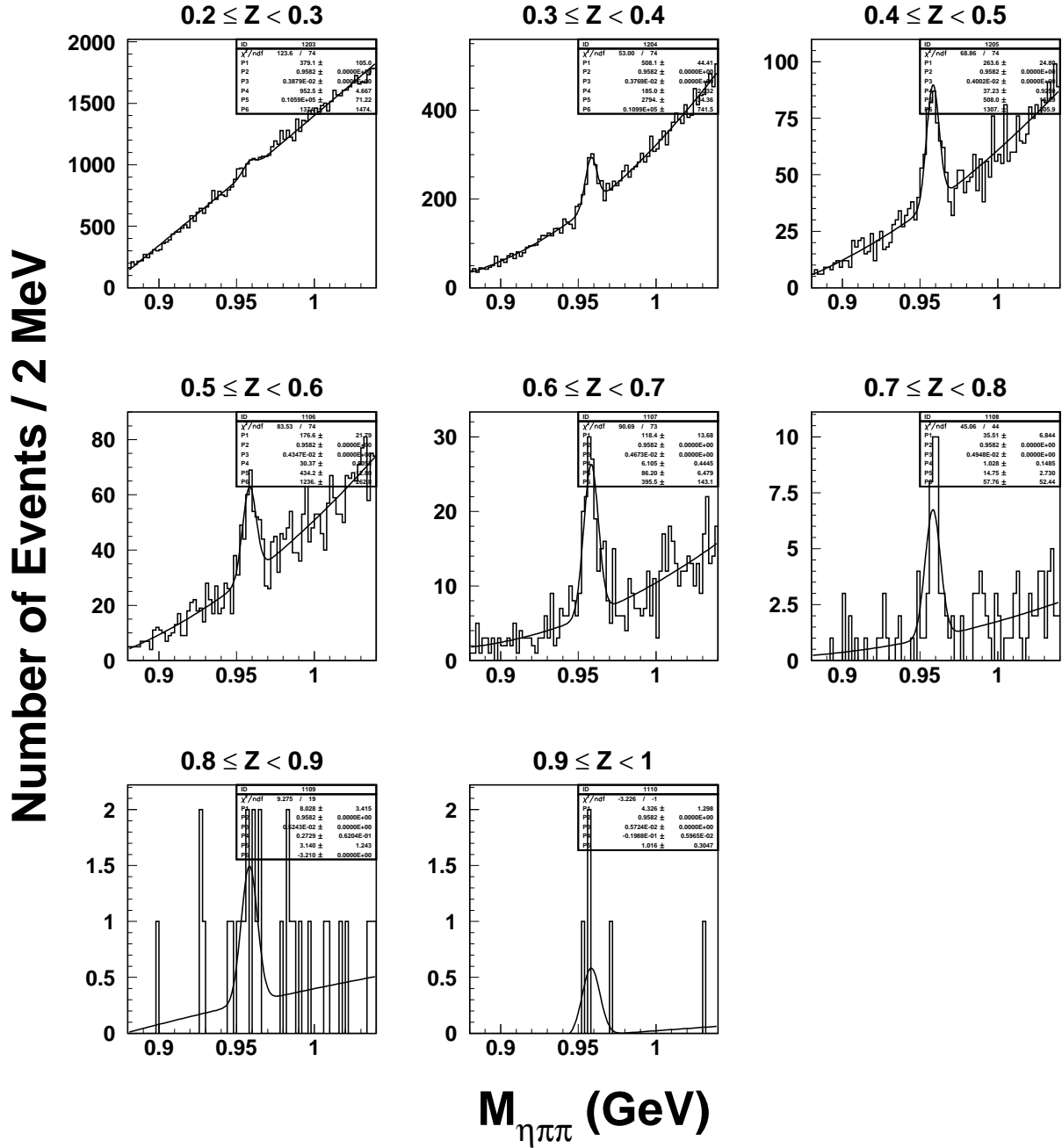


Figure 4: The $\eta\pi^+\pi^-$ invariant mass spectra in different Z ranges reconstructed from $\Upsilon(1S)$ data, fit with Gaussian function for signal and second order polynomial for background.

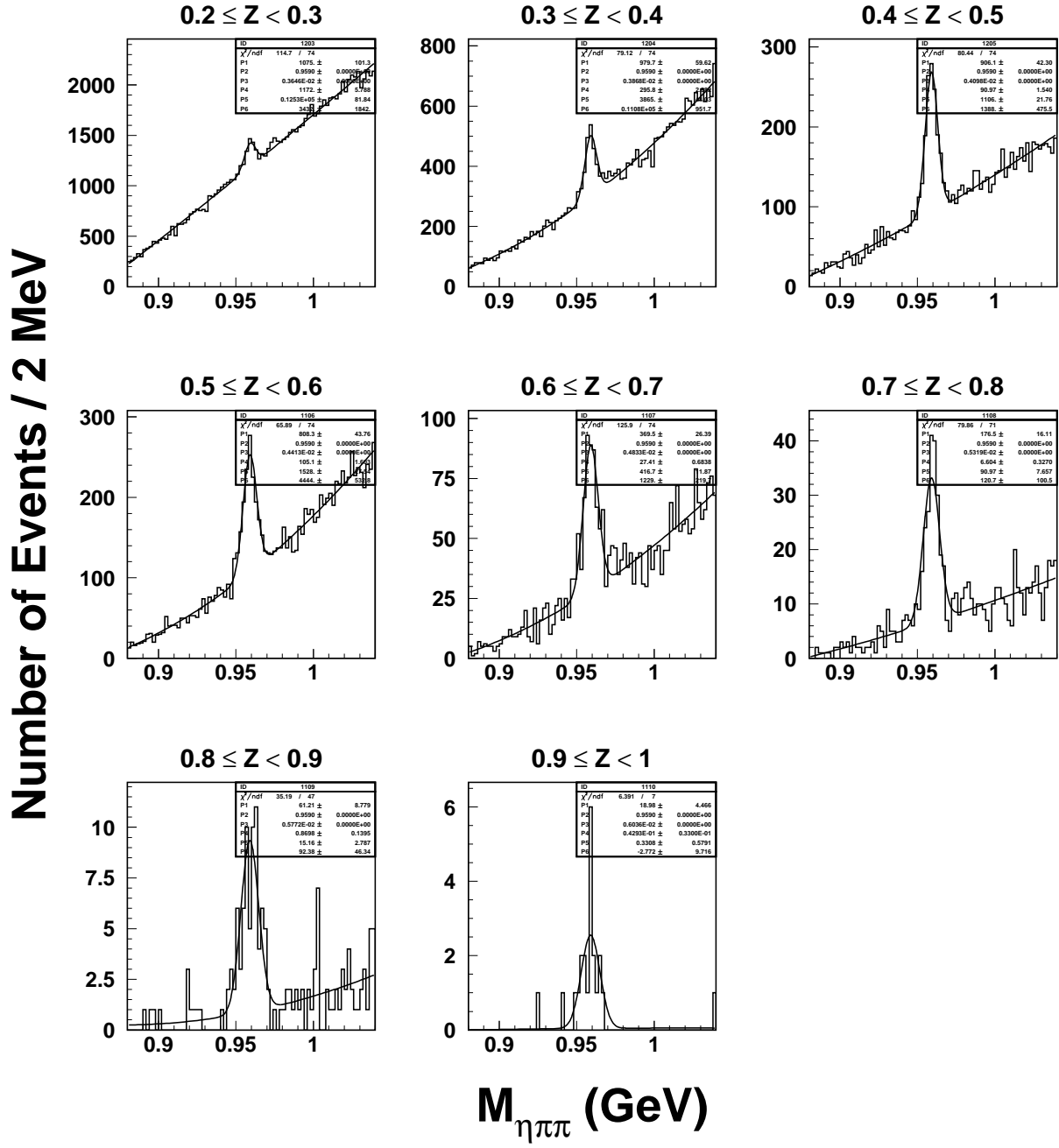


Figure 5: The $\eta\pi^+\pi^-$ invariant mass spectra in different Z ranges reconstructed from off-resonance data, fit with Gaussian function for signal and second order polynomial for background.

GeV) and dashed line for the continuum data ($E_{\text{CM}} = 10.52$ GeV). The low limits are 0.202 and 0.182 respectively. The discrepancy is significant, especially at low energy. In order to use our continuum data at 10.52 GeV we need to map it to 9.46 GeV. To do so we rely on the continuum Monte Carlo. We take the two Monte Carlo η' shape distributions at 10.52 and 9.46 GeV, denoted by $\mathcal{P}_{10.52}(z)$ and $\mathcal{P}_{9.46}(z)$ and numerically integrate them to satisfy the relation:

$$\int_0^{Z'_{10.52}} \mathcal{P}_{10.52}(z) dz = \int_0^{Z'_{9.46}} \mathcal{P}_{9.46}(z) dz \quad , \quad (4)$$

where $Z'_{10.52}$ is fixed and a value for $Z'_{9.46}$ is determined. The data points on Figure 6-(b) show the difference in $Z'_{9.46} - Z'_{10.52}$ as a function of $Z'_{10.52}$ (or equivalently Z_0 in following function). We fit the points with a fourth order polynomial function to define the mapping analytically as

$$Z = -0.215 \times 10^{-2} + 1.2238 Z_0 - 0.6879 Z_0^2 + 0.8277 Z_0^3 - 0.3606 Z_0^4 \quad . \quad (5)$$

The simplest mapping would be a linear conversion $Z = 0.025 + 0.975 \times Z_0$, shown as dotted line in Figure 6-(b). We use this alternative to estimate the systematic error due to the mapping.

That this mapping works, is demonstrated in Figure 6-(a), where the spectra shown as open circles is the mapped spectrum according to equation 5. It overlaps well with the Monte Carlo spectrum generated at 9.46 GeV.

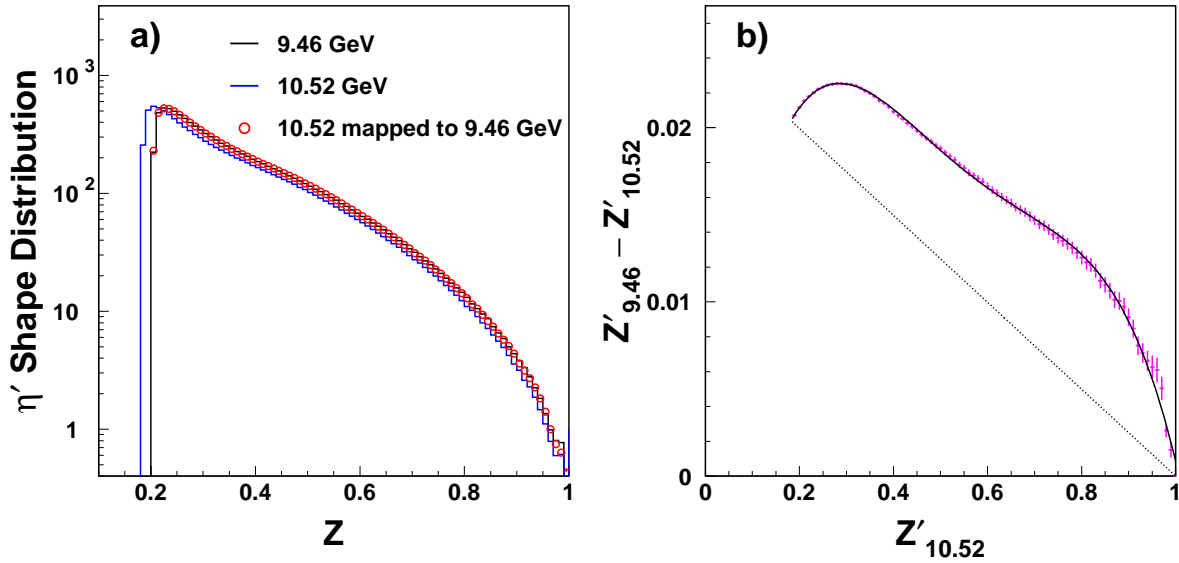


Figure 6: a) The $Z = E_{\eta'}/E_{beam}$ distributions from Monte Carlo simulation. The solid line is the $Z=E_{\eta'}/E_{beam}$ spectrum for an energy of 9.46 GeV, the dashed line is the spectrum for 10.52 GeV and the open circles are the mapped spectrum from 10.52 GeV. b) The data points show the difference in the Z values at 9.46 and 10.52 GeV as a function of the Z value at 10.46 GeV. The solid curve is a fit to a fourth order polynomial. The dotted line is the mapping of linear conversion.

The η' production rate is smaller at 9.46 GeV due to less available energy. From the $q\bar{q}$ generator we found that the production rate is 93.6% that of 10.52 GeV. This factor is considered in estimation of the η' production from $q\bar{q}$ events.

The mapping for continuum data is derived from the model-dependent Monte Carlo spectrum. If the real data and the Monte Carlo are very different then a systematic error due to this mapping could be large. To check this, we compared the measured $E_{\eta'}/E_{\text{beam}}$ spectrum with the generated spectrum. Fortunately, the spectra agree reasonably well and the systematic error due to this source is negligible.

We now turn to estimating the detection efficiencies. Shown in Figure 7 are the efficiencies estimated with different models and different energies for a) without the π^0 veto, and b) with the π^0 veto. In the real data we applied π^0 veto to η' candidates with $Z < 0.5$. Comparing with the efficiency from 9.46 GeV $q\bar{q}$ events, the efficiency from ggg events is roughly 15% higher, and the efficiency from 10.52 GeV $q\bar{q}$ events is roughly 7% lower. The main source of such difference is the event shape. The ggg event are more spherical while the higher energy $q\bar{q}$ events are more jetty.

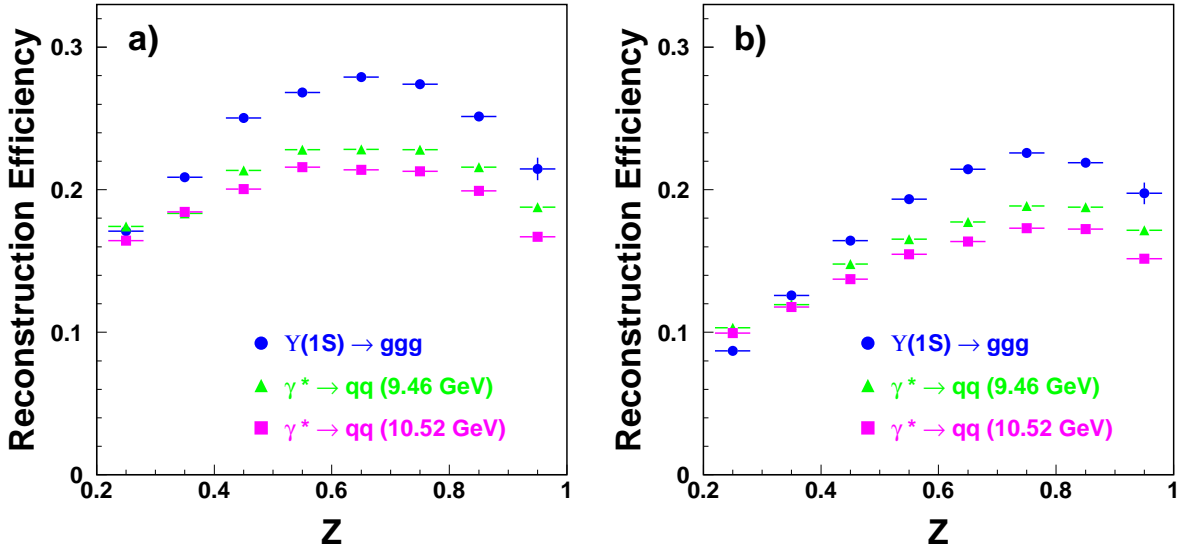


Figure 7: The η' reconstruction efficiencies as function of Z for different MC samples a) with no π^0 veto, and b) with π^0 veto in photon selection.

4 Results

The $Y(1S)$ data sample can be broken down into three parts as described in previous section:

$$N_{all} = N_{Y(1S) \rightarrow ggg} + N_{Y(1S) \rightarrow q\bar{q}} + N_{e^+e^- \rightarrow \gamma^* \rightarrow q\bar{q}}.$$

The first one has different reconstruction efficiencies from the other two. For the contribution from continuum ($\gamma^* \rightarrow q\bar{q}$) events, we multiply the number from off-resonance events, suitably

mapped, by a factor $f_{\gamma^* \rightarrow q\bar{q}}$ which can be found as:

$$N(\eta')_{\gamma^* \rightarrow q\bar{q}}(9.46 \text{ GeV}) = N(\eta')_{\gamma^* \rightarrow q\bar{q}}(10.52 \text{ GeV}) \times f_{\gamma^* \rightarrow q\bar{q}}, \quad (6)$$

where

$$\begin{aligned} f_{\gamma^* \rightarrow q\bar{q}} &= \frac{80.4}{1192.9} \times \frac{1/9.46^2}{1/10.52^2} \times 0.9356 \times \frac{\epsilon_{9.46}}{\epsilon_{10.52}} \\ &= 0.0780 \times \frac{\epsilon_{9.46}}{\epsilon_{10.52}}, \end{aligned} \quad (7)$$

where the first term is the relative luminosities, the second the energy squared dependence of the cross section, the third the relative η' yield and ϵ is the Z -dependent reconstruction efficiency for $q\bar{q}$ events as shown Figure 7.

We also want to evaluate the yield from $\Upsilon(1S) \rightarrow \gamma \rightarrow q\bar{q}$ Since we know that $\sigma_{\Upsilon(1S) \rightarrow \mu^+ \mu^-} = 0.555 \pm 0.022 \text{ nb}$ and $\sigma_{\gamma^* \rightarrow \mu^+ \mu^-}(9.46 \text{ GeV}) = 1.12 \text{ nb}$ [10], we can easily derive the factor to be used for $N_{\Upsilon(1S) \rightarrow q\bar{q}}$ estimation:

$$\begin{aligned} f_{\Upsilon(1S) \rightarrow q\bar{q}} &= f_{\gamma^* \rightarrow q\bar{q}} \times \frac{R \cdot \sigma_{\Upsilon(1S) \rightarrow \mu^+ \mu^-}}{R \cdot \sigma_{\gamma^* \rightarrow \mu^+ \mu^-}} \\ &= 0.0387 \times \frac{\epsilon_{9.46}}{\epsilon_{10.52}}. \end{aligned} \quad (8)$$

In Table 2 we list the number of reconstructed η' over all Z and in the high Z region for various $\Upsilon(1S)$ and continuum yields (only statistical errors are shown). Note that the total numbers of signal from $\Upsilon(1S)$ data and off-resonance data in this table are the sum of all Z bins derived bin per bin, as we need to use Z -dependent efficiencies. The numbers are different from the yields in Figures 2 and 3. The difference will be considered in systematic error estimation.

Sample	All Z	$Z > 0.7$
$\Upsilon(1S)$ data	1494 ± 120	46.0 ± 8.1
off-resonance	4294 ± 130	257.1 ± 17.3
$\Upsilon(1S) \rightarrow ggg$	972 ± 120	13.9 ± 8.1
$\Upsilon(1S) \rightarrow q\bar{q}$	173 ± 5	10.6 ± 0.7
Continuum $q\bar{q}$	349 ± 11	21.5 ± 1.4
$\Upsilon(1S) \rightarrow ggg, q\bar{q}$	1145 ± 120	24.5 ± 8.1

Table 2: Number of reconstructed η' from $\Upsilon(1S)$ and off-resonance data and the breakdown categories of $\Upsilon(1S)$ data. Also listed are for samples with $Z > 0.7$.

We measure the $\Upsilon(1S) \rightarrow \eta' X$ branching fractions as:

$$\begin{aligned} \mathcal{B}(\Upsilon(1S) \rightarrow \eta' X) &= (2.8 \pm 0.4 \pm 0.2)\%, \\ \mathcal{B}(\Upsilon(1S) \rightarrow (ggg) \rightarrow \eta' X) / \mathcal{B}(\Upsilon(1S) \rightarrow (ggg)) &= (2.8 \pm 0.5 \pm 0.2)\%, \\ \mathcal{B}(\Upsilon(1S) \rightarrow (q\bar{q}) \rightarrow \eta' X) / \mathcal{B}(\Upsilon(1S) \rightarrow (q\bar{q})) &= (4.2 \pm 0.2 \pm 0.4)\%. \end{aligned} \quad (9)$$

We now consider the systematic errors. We assign errors of $\pm 2.2\%$ on the reconstruction efficiency of each charged track, and $\pm 5\%$ for the η . The number of reconstructed η' are extracted from fit. We assign $\pm 2\%$ error to this source. The total number of $\Upsilon(1S)$ has a relative error of $\pm 2.4\%$. The branching fraction of $\eta' \rightarrow \pi^+\pi^-\eta$ introduces $\pm 3.4\%$ error. In calculating the branching fraction in the $q\bar{q}$ sample, we used branching fraction $\mathcal{B}(\Upsilon(1S) \rightarrow (q\bar{q})) = (8.83 \pm 0.28)\%$. The relative error is $\pm 3.2\%$. We use the ratio of integrated luminosities of $\Upsilon(1S)$ and off-resonance data in calculating $f_{\gamma^* \rightarrow q\bar{q}}$ and $f_{\Upsilon(1S) \rightarrow q\bar{q}}$. The uncertainty of this ratio is about $\pm 1\%$ [11]. The uncertainty of $\sigma_{\Upsilon(1S) \rightarrow \mu^+\mu^-}$ is about 4% which also affects $f_{\Upsilon(1S) \rightarrow q\bar{q}}$. These latter two directly affect the branching fraction in the $q\bar{q}$ sample with error of 1% and 4% respectively. The effects of these two sources to the overall and the ggg sample branching fractions are negligible except for the branching fraction measurement of high energy η' in the ggg samples, there are $\pm 2.9\%$ and $\pm 3.6\%$ uncertainties. The Z mapping results in $\pm 3\%$ errors on all branching fractions except for $Z > 0.7$ for the ggg sample where a $\pm 6\%$ error is assigned. The systematic errors are summarized in Table 3. The total systematic errors on branching ratios are $\pm 10\%$ for $q\bar{q}$ sample, $\pm 11\%$ for ggg sample at $Z > 0.7$, and $\pm 8.6\%$ for the rest.

Sources	ggg Sample ($Z > 0.7$)	$q\bar{q}$ Sample	All others
Reconstruction efficiency of π^\pm	4.4	4.4	4.4
Reconstruction efficiency of η	5	5	5
Number of η' from fit	2	2	2
Total number of $\Upsilon(1S)$	2.4	2.4	2.4
$\mathcal{B}(\eta' \rightarrow \pi^+\pi^-\eta)$	3.4	3.4	3.4
$\mathcal{B}(\Upsilon(1S) \rightarrow q\bar{q})$	-	3.2	-
Ratio of integrated luminosity	2.9	1	-
$\sigma_{\Upsilon(1S) \rightarrow \mu^+\mu^-}$	3.6	4	-
Z mapping	6	3	3
Total	11	10	8.6

Table 3: The systematic errors in percentage on branching fraction measurements from different sources.

The $\Upsilon(1S) \rightarrow \eta' X$ branching fractions at high momentum ($Z > 0.7$) are measured to be:

$$\begin{aligned}
\mathcal{B}(\Upsilon(1S) \rightarrow \eta' X)_{Z>0.7} &= (3.1 \pm 0.9 \pm 0.3) \times 10^{-4}, \\
\mathcal{B}(\Upsilon(1S) \rightarrow (ggg) \rightarrow \eta' X)_{Z>0.7} / \mathcal{B}(\Upsilon(1S) \rightarrow (ggg)) &= (1.9 \pm 1.1 \pm 0.2) \times 10^{-4}, \\
\mathcal{B}(\Upsilon(1S) \rightarrow (q\bar{q}) \rightarrow \eta' X)_{Z>0.7} / \mathcal{B}(\Upsilon(1S) \rightarrow (q\bar{q})) &= (16.8 \pm 1.1 \pm 1.7) \times 10^{-4}. \quad (10)
\end{aligned}$$

At 90% confidence level, we derive an upper limit of $\mathcal{B}(\Upsilon(1S) \rightarrow (ggg) \rightarrow \eta' X)_{Z>0.7} / \mathcal{B}(\Upsilon(1S) \rightarrow (ggg))$ to be 3.4×10^{-4} .

We also measured the differential branching fraction as a function of Z as shown in Figure 8. In the plots only statistic error is shown which dominates the total error. There is about 10% systematic error which does not change the shape of distribution. We define three relevant differential branching ratio's dn/dZ as:

$$\frac{dn(ggg)}{dZ} = \frac{d\mathcal{B}(\Upsilon(1S) \rightarrow (ggg) \rightarrow \eta' X)}{dZ \times \mathcal{B}(\Upsilon(1S) \rightarrow (ggg))},$$

$$\frac{dn(q\bar{q})}{dZ} = \frac{dB(\Upsilon(1S) \rightarrow (q\bar{q}) \rightarrow \eta' X)}{dZ \times B(\Upsilon(1S) \rightarrow (q\bar{q}))} ,$$

$$\frac{dn(1S)}{dZ} = \frac{dB(\Upsilon(1S) \rightarrow \eta' X)}{dZ} . \quad (11)$$

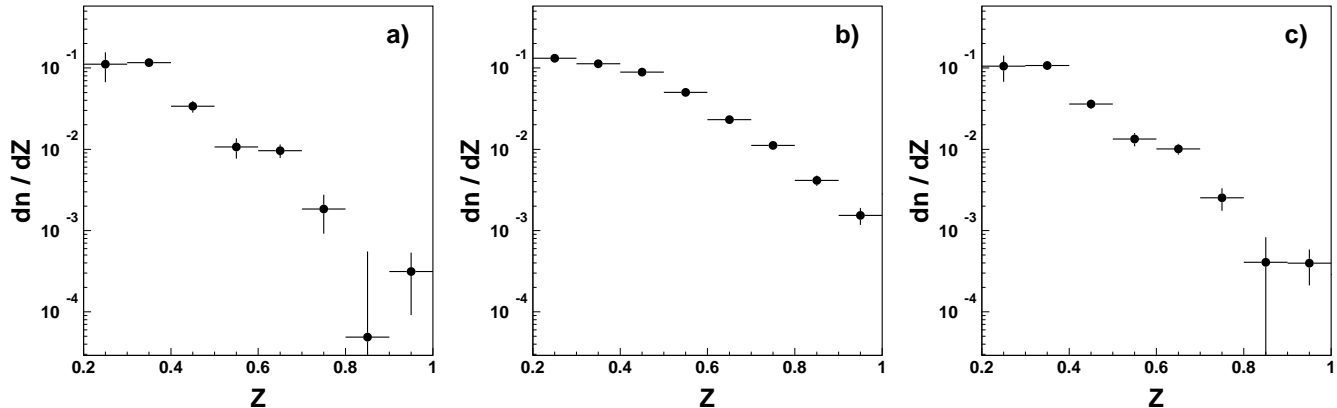


Figure 8: The differential branching fraction dn/dZ as defined in context for a) $\Upsilon(1S) \rightarrow ggg \rightarrow \eta' X$, b) $\Upsilon(1S) \rightarrow q\bar{q} \rightarrow \eta' X$, and c) $\Upsilon(1S) \rightarrow \eta' X$.

In the Z spectrum of η' produced via ggg , there is a significant excess above an apparent exponential decrease for $0.6 < Z < 0.7$, corresponding to a recoil mass opposite the η' in the range 5.3 to 6.1 GeV. However, a detailed study did not reveal any narrow structures. A possible explanation is that there is more than one processes contributing to this distribution. We note also that the $q\bar{q}$ has much larger rates at high Z than ggg .

5 Comparison with theoretical predictions

Figure 9 shows Z spectrum of the η' measured in this paper compared with the spectra predicted by the three different models mentioned above. The measurement strongly favors rapidly falling q^2 dependence of the $g^* g \eta'$ form factor predicted by pQCD[12], and ruling out other models. However, it again appears that there is more than one process present.

6 Acknowledgements

We thank Alex Kagan for useful discussions on the theoretical models. We thank Rich Galik, David Kreinick on suggestions on 1S data, and Brian Heltsley on luminosity issues.

References

- [1] T. E. Browder *et al.* [CLEO Collaboration], Phys. Rev. Let. **81**, 1786 (1998), [hep-ex/9804018]

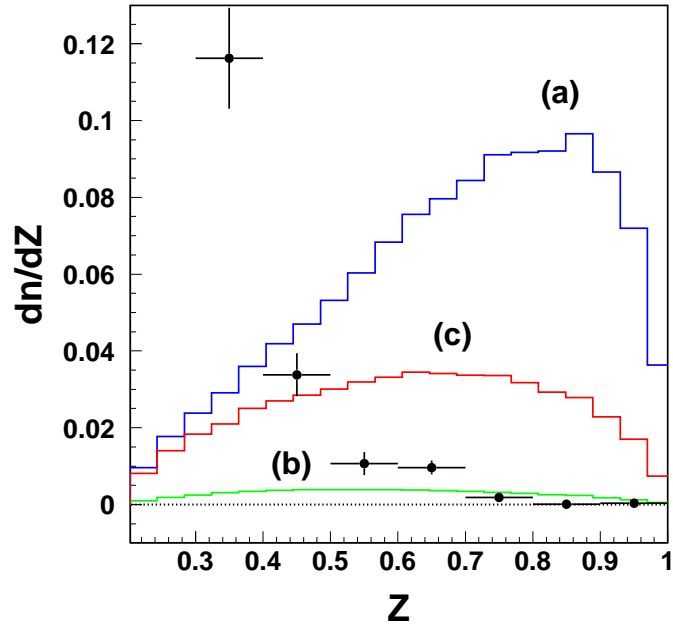


Figure 9: The measured dn/dZ spectrum of $\Upsilon(1S) \rightarrow (ggg) \rightarrow \eta'X$ compared with theoretical predictions. Shown in dots are the measurement in this study. Shown in lines are different theoretical predictions: a) a slowly falling form factor, b) a rapidly falling form factor, and c) intermediate form factor [5]).

- [2] D. Atwood and A. Soni, Phys. Lett. B **405**, 150 (1997) [hep-ph/9704357].
- [3] W. S. Hou and B. Tseng, Phys. Rev. Lett. **80**, 434 (1998) [hep-ph/9705304].
- [4] A. Kagan, [hep-ph/9806266].
- [5] A. L. Kagan, [hep-ph/0201313]
- [6] A. Ali and A. Y. Parkhomenko, Phys. Rev. D **65**, 074020 (2002) [arXiv:hep-ph/0012212].
- [7] R. Ammar *et al.* [CLEO Collaboration], Phys. Rev. D **57**, 1350 (1998) [hep-ex/9707018].
- [8] A. Zimmermann, Diplom Thesis, University of Dortmund, April 1992; see also ARGUS collaboration, Z. Phys. C **58**, 1199-206 (1993).
- [9] V. Fadeyev *et al.*, CBX 98-16.
- [10] W. Y. Chen *et al.*, Phys. Rev. D **39**, 3528 (1989).
- [11] Although the luminosity measurement at $\Upsilon(1S)$ is not as well studied as at $\Upsilon(4S)$ due to the e^+e^- pairs from $\Upsilon(1S)$ decay, Brian Heltsley thought that 1% error on the integrated luminosity ratio in this study is a reasonable.
- [12] T. Muta and M. Z. Yang, Phys. Rev. D **61**, 054007 (2000) [hep-ph/9909484], A. Ali and A. Y. Parkhomenko, Phys. Rev. D **65**, 074020 (2002) [hep-ph/0012212].

7 Appendix: Some useful tables and plots

The reconstruction efficiency for different Z intervals using three different MC samples is shown in Table 4. The number with no π^0 veto or with π^0 veto in photon selection are listed. In other plots or tables we use π^0 veto for samples with $Z < 0.5$ and no π^0 veto for the rest.

In Table 5 we list the number of reconstructed η' in different Z intervals using on-resonance $\Upsilon(1S)$ data (1S1, 1S2, and 1S3 datasets), and off-resonance $\Upsilon(4S)$ data (4S2-4S7, 4SE-4SG datasets). Also listed are the number of breakdown categories from $\Upsilon(1S)$ data where we use off-resonance $\Upsilon(4S)$ data to estimate the contributions from $q\bar{q}$ type of categories. We also list the total number of reconstructed η' for all Z range and for $Z > 0.7$.

The breakdown of η' spectrum from $\Upsilon(1S)$ data is shown in Figure 10, where the reconstruction efficiency is corrected and production cross-sections are calculated.

Table 6 shows the number of reconstructed η' with reconstruction efficiency corrected. In Figure 7 and Table 4 we show the reconstruction efficiency of the dedicated decay chain. In this table the branching fractions are considered and thus it represents overall η' production.

Listed in Table 7 is the differential branching fraction to inclusive η' . The branching fractions of sub-samples: ggg and $q\bar{q}$ are to the total number of $\Upsilon(1S)$ in that sample, while the branching fraction in column “All $\Upsilon(1S)$ ” are to all $\Upsilon(1S)$ including di-leptonic events. Also listed are total branching fractions with η' in all Z ranges and $Z > 0.7$.

Z	$\Upsilon(1S) \rightarrow (ggg) \rightarrow \eta' X$ $\sqrt{s} = 9.46 \text{ GeV}$	$\Upsilon(1S) \rightarrow (q\bar{q}) \rightarrow \eta' X$ $\sqrt{s} = 9.46 \text{ GeV}$	$\Upsilon(1S) \rightarrow (q\bar{q}) \rightarrow \eta' X$ $\sqrt{s} = 10.52 \text{ GeV}$
Without π^0 photon rejection			
0.2 - 0.3	0.170 ± 0.003	0.173 ± 0.003	0.165 ± 0.003
0.3 - 0.4	0.206 ± 0.002	0.182 ± 0.003	0.184 ± 0.003
0.4 - 0.5	0.249 ± 0.002	0.213 ± 0.003	0.201 ± 0.003
0.5 - 0.6	0.268 ± 0.002	0.228 ± 0.003	0.217 ± 0.003
0.6 - 0.7	0.279 ± 0.002	0.228 ± 0.003	0.215 ± 0.003
0.7 - 0.8	0.273 ± 0.003	0.227 ± 0.002	0.214 ± 0.002
0.8 - 0.9	0.251 ± 0.003	0.215 ± 0.002	0.200 ± 0.001
0.9 - 1.0	0.215 ± 0.008	0.188 ± 0.003	0.167 ± 0.002
With π^0 photon rejection			
0.2 - 0.3	0.087 ± 0.002	0.103 ± 0.002	0.100 ± 0.002
0.3 - 0.4	0.125 ± 0.002	0.118 ± 0.002	0.118 ± 0.002
0.4 - 0.5	0.164 ± 0.002	0.147 ± 0.002	0.138 ± 0.002
0.5 - 0.6	0.193 ± 0.002	0.165 ± 0.002	0.156 ± 0.002
0.6 - 0.7	0.214 ± 0.002	0.177 ± 0.002	0.164 ± 0.002
0.7 - 0.8	0.225 ± 0.003	0.188 ± 0.002	0.174 ± 0.002
0.8 - 0.9	0.218 ± 0.003	0.187 ± 0.002	0.173 ± 0.002
0.9 - 1.0	0.198 ± 0.008	0.172 ± 0.002	0.152 ± 0.002

Table 4: The reconstruction efficiency of η' for different Z intervals and different samples.

Z	On-resonance $\Upsilon(1S)$ data	Off-resonance $\Upsilon(4S)$ data	Breakdown of $\Upsilon(1S)$ data		
			$\Upsilon(1S) \rightarrow (ggg)$	$\Upsilon(1S) \rightarrow (q\bar{q})$	$\gamma^* \rightarrow (q\bar{q})$
0.2 - 0.3	379.1 ± 105.0	973.8 ± 92.4	262.1 ± 105.0	38.8 ± 3.7	78.2 ± 7.4
0.3 - 0.4	508.1 ± 44.4	979.7 ± 59.6	393.0 ± 44.4	38.2 ± 2.3	77.0 ± 4.7
0.4 - 0.5	263.6 ± 24.8	906.1 ± 42.3	150.3 ± 24.8	37.6 ± 1.8	75.8 ± 3.5
0.5 - 0.6	176.6 ± 21.8	808.3 ± 43.8	77.6 ± 21.8	32.8 ± 1.8	66.2 ± 3.6
0.6 - 0.7	118.4 ± 13.7	369.5 ± 26.4	72.8 ± 13.7	15.1 ± 1.1	30.5 ± 2.2
0.7 - 0.8	35.5 ± 6.8	176.5 ± 16.1	13.6 ± 6.8	7.3 ± 0.7	14.6 ± 1.3
0.8 - 0.9	8.0 ± 3.4	61.2 ± 8.8	0.3 ± 3.4	2.6 ± 0.4	5.1 ± 0.7
0.9 - 1.0	4.3 ± 1.3	19.0 ± 4.5	1.8 ± 1.3	0.8 ± 0.2	1.7 ± 0.4
0.7 - 1.0	46.0 ± 8.1	257.1 ± 17.3	13.9 ± 8.1	10.6 ± 0.7	21.5 ± 1.4
sum of all	1494 ± 120	4294 ± 130	972 ± 120	173 ± 5	349 ± 11

Table 5: Number of reconstructed η' in different Z intervals and from different samples.

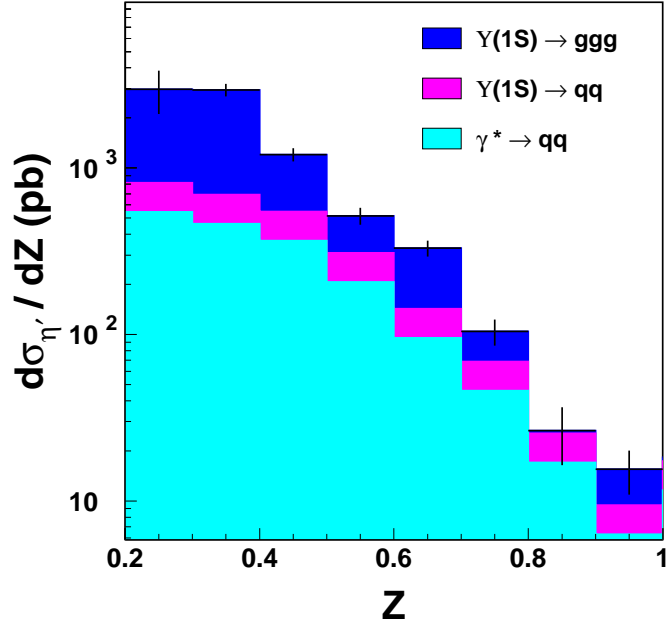


Figure 10: The breakdown of η' spectrum from $\Upsilon(1S)$ data.

Z	$\Upsilon(1S) \rightarrow (ggg)$	$\Upsilon(1S) \rightarrow (q\bar{q})$	$\gamma^* \rightarrow (q\bar{q})$	$\Upsilon(1S) \rightarrow (ggg, q\bar{q})$
0.2 - 0.3	17384.7 ± 6962.7	2170.8 ± 206.1	4376.4 ± 415.4	19555.6 ± 6962.7
0.3 - 0.4	18101.3 ± 2045.5	1849.6 ± 112.5	3728.8 ± 226.9	19950.9 ± 2045.5
0.4 - 0.5	5265.5 ± 868.8	1462.9 ± 68.3	2949.2 ± 137.7	6728.4 ± 868.8
0.5 - 0.6	1660.8 ± 466.5	826.9 ± 44.8	1667.0 ± 90.2	2487.6 ± 466.5
0.6 - 0.7	1500.2 ± 281.9	381.6 ± 27.3	769.4 ± 54.9	1881.8 ± 281.9
0.7 - 0.8	286.5 ± 143.9	183.5 ± 16.8	369.9 ± 33.8	470.0 ± 143.9
0.8 - 0.9	7.6 ± 78.2	68.1 ± 9.8	137.4 ± 19.7	75.7 ± 78.2
0.9 - 1.0	48.8 ± 34.6	25.2 ± 5.9	50.8 ± 12.0	74.0 ± 34.6
0.7 - 1.0	301.7 ± 175.3	276.5 ± 18.6	557.4 ± 37.5	578.2 ± 175.3
sum of all	44255.4 ± 7331.0	6968.6 ± 250.9	14048.9 ± 505.8	51224.0 ± 7331.0

Table 6: Number of reconstructed η' in different Z intervals after efficiency correction where the branching fraction is taken into consideration.

Z	$\Upsilon(1S) \rightarrow (ggg)$	$\Upsilon(1S) \rightarrow (q\bar{q})$	All $\Upsilon(1S)$
0.2 - 0.3	11163.8 ± 4471.2	13204.6 ± 1253.4	10503.4 ± 3739.7
0.3 - 0.4	11623.9 ± 1313.6	11250.4 ± 684.6	10715.7 ± 1098.7
0.4 - 0.5	3381.3 ± 557.9	8898.4 ± 415.5	3613.8 ± 466.6
0.5 - 0.6	1066.5 ± 299.6	5029.6 ± 272.3	1336.1 ± 250.6
0.6 - 0.7	963.4 ± 181.1	2321.3 ± 165.8	1010.7 ± 151.4
0.7 - 0.8	184.0 ± 92.4	1116.2 ± 101.9	252.4 ± 77.3
0.8 - 0.9	4.9 ± 50.2	414.5 ± 59.4	40.7 ± 42.0
0.9 - 1.0	31.3 ± 22.2	153.3 ± 36.1	39.7 ± 18.6
0.7 - 1.0	19.4 ± 11.3	168.2 ± 11.3	31.1 ± 9.4
sum of all	2841.9 ± 470.8	4238.8 ± 152.6	2751.3 ± 393.8

Table 7: Differential braching fraction of η' ($\times 10^{-5}$). The last two rows are total braching fractions. The braching fractions in columns 2 and 3 are normalized to the total branching fraction of $\Upsilon(1S) \rightarrow (ggg)$ and $\Upsilon(1S) \rightarrow (q\bar{q})$ respectively, while the last column is to all $\Upsilon(1S)$.